© 2022 IEEE. Personal use of this material is permitted. Permission from IEEE must be obtained for all other uses, in any current or future media, including reprinting/republishing this material for advertising or promotional purposes,creating new collective works, for resale or redistribution to servers or lists, or reuse of any copyrighted component of this work in other works.

UNTANGLING THE GNSS-R COHERENT AND INCOHERENT COMPONENTS: EXPERIMENTAL EVIDENCES OVER THE OCEAN

J.F. Munoz-Martin[1], R. Onrubia , D. Pascual , H. Park[1], A. Camps[1],
C. Rüdiger[2], J. Walker[2], and A. Monerris[3]

[1]CommSensLab - UPC, Universitat Politècnica de Catalunya – BarcelonaTech, and IEEC/CTE-UPC
[2]Department of Civil Engineering, Monash University, Clayton, VIC 3800, Australia
[3]Department of Infrastructure Engineering, The University of Melbourne, Parkville, VIC 3010, Australia,
e-mail: joan.francesc@tsc.upc.edu, camps@tsc.upc.edu

ABSTRACT

Global Navigation Satellite Systems Reflected (GNSS-R) signals exhibit an incoherent and a coherent components [1, 2]. Current models assume that one or the other are dominant, and the calibration, and geophysical parameter retrieval (eg. wind speed, soil moisture...) are developed accordingly. Even the presence itself of the coherent component of a GNSS reflected signal has been a matter of discussion in the last years. In this work, the method used in [3] to separate the leakage of the direct signal from the reflected one is applied to a set of GNSS signals reflected collected over the ocean by the MIR [4, 5], an airborne dual-band (L1/E1 and L5/E5a), multi-constellation (GPS and Galileo) GNSS-R instrument with two 19-elements array with 4 beam-steered each.

The results presented demonstrate the feasibility of the proposed technique to untangle the coherent and incoherent components in GNSS reflected signals. This technique allows the processing of these components separately, which will increase the calibration accuracy (as today both are mixed together), and allows high resolution applications since the spatial resolution of the coherent component is determined by the size of the first Fresnel zone [6] (300-500 meters from a LEO satellite), and not by the size of the glistening zone (~25 km from a LEO satellite).

Index Terms— GNSS-R, Sea, Coherent scattering, incoherent scattering

1. INTRODUCTION

The Microwave Interferometric Reflectometer (MIR) [4, 7] is an airborne GNSS-R instrument conceived to perform cGNSS-R and iGNSS-R using dual-band (L1/E1 and L5/E5a) high directive up-looking and down-looking antenna arrays (~21 dB at L1, ~18 dB at L5). Despite the instrument was conceived for real-time processing, the 1-bit raw data sampled at 32 MS/s is also stored as part of the observables, to test other techniques offline. MIR maiden flights were conducted

in Victoria, Australia in 2018. One of the flights was conducted over the Bass Strait, the area that separates Australia and Tasmania. The large directivity of the MIR antennas allows a very clear detection of the GNSS reflected signal with short incoherent integration times (40-300 ms). Despite the evidences shown in the phase of the Delay-Doppler Map (DDM) over the ocean [8], and over land [9] during the last years, there have been many discussions on the presence or not of a coherent component in the GNSS reflected signal and its magnitude.

This work analyzes in more depth the presence of a coherent component with new data coming from MIR instrument. The large directivity allows a higher signal-to-noise ratio and hence an improved detection of the coherent component with shorter integration times.

The data under analysis corresponds to a flight over the Bass Strait on June 6^{th}, 2018. The plane was flying at a height of 1500 meters at an average speed of 74 m/s. The data used corresponds to three passes following a line going from 37.9ºS, 149,23ºE to 38.9ºS, 149.1ºE, as shown in Fig. 1. The GNSS-R data used include both L1/E1 and L5/E5a bands and also contain data from both GPS and Galileo constellations at different incidence angles.

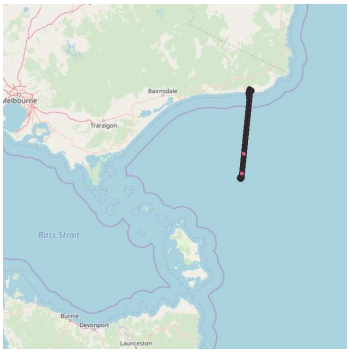

Fig. 1: Flight path on June 6^{th}, 2018 associated to the data used for the coherent/incoherent component untangling

2. COHERENCY OF THE CGNSS-R SIGNAL

In the conventional GNSS-R technique the reflected signal is correlated with a perfect replica of the GNSS code generated on the receiver [10]. In [3] a method was proposed to detect and eliminate the direct signal. In this work, it is proposed to use the same technique to detect the coherent component present in a GNSS-R signal [11].

The technique explained in [3] consists of the computation of the variance of the coherently integrated DDM (Y, as shown in Eq. 1), i.e. prior to the incoherent averaging, as in (2).

$$Y_i(\tau,\nu) = \frac{1}{T_c}\int_{iT_c}^{(i+1)T_c} x(t)y^*(t-\tau)e^{-j2\pi\nu t}dt \quad (1)$$

$$Var(Y) = E[|Y|^2] - |E[Y]|^2, \quad (2)$$

Where $E[|Y|^2]$ is the incoherently averaged DDM. In practice, the variance term, $Var(Y)$ is computed as the mean square of the N_{inc} samples (amount of samples incoherently averaged) minus the arithmetic mean of the samples (μ), as in Eq. 3a.

$$Var(Y) = \frac{1}{N_{inc}}\sum_{i=1}^{N_{Inc}} |Y_i - \mu|^2 \quad (3a)$$

$$\mu = \frac{1}{N_{inc}}\sum_{i=1}^{N_{Inc}} Y_i \quad (3b)$$

The difference of (2) and (3a) gives the coherent component averaged over N_{inc} samples, as shown in Eq. 4.

$$|E[Y]|^2 = \frac{1}{N_{inc}}\sum_{i=1}^{N_{inc}} |Y_i|^2 - \frac{1}{N_{inc}}\sum_{i=1}^{N_{inc}} |Y_i - \mu|^2$$

3. RESULTS

In order to characterize and classify the waveforms, a ratio between the coherent component and the total incoherent averaging is used: the coherent component to incoherent ratio (CIR), as defined in (5). As an example, the direct GNSS signal has a CIR = 1, as is completely coherent.

$$CIR = \frac{|E[Y]|^2}{E[|Y|^2]} \quad (5)$$

To illustrate the coherent and incoherent component untangling, two different waveforms ($Y_{\tau,f_d} = 0$) have been selected for each signal type: GPS L1CA, GPS L5, Galileo E1, and Galileo E5a.

Fig. 2 shows two waveforms for GPS L1CA case with an incidence angle of 21° and 30°, respectively. The first waveform shows a very high CIR = 0.83, indicating that the waveform has a very strong coherent component, while the second waveform, with a larger incidence angle, presents a lower CIR.

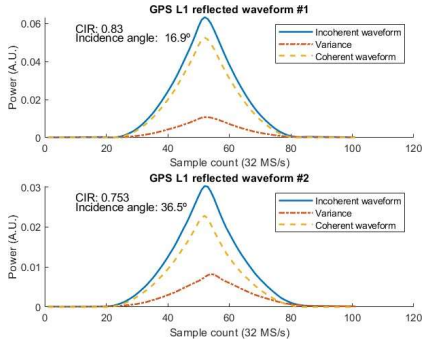

Fig. 2: Incoherent component, variance, and coherent component of GPS L1 reflected signal

The second case is the Galileo E1 in which, as opposed to the GPS L1CA case, it is not enough data to show waveforms collected with different incidence angles, as the tracking of the Galileo E1 signal of this flight was limited to a couple of minutes. Despite that, both waveforms present similar CIR (0.63 and 0.58 respectively, as shown in Fig. 3), this ratio is lower than the GPS L1CA at the same incidence angle. The decrease of CIR for the incidence angle can come for the difference in the natural correlation time of the Galileo E1 signal versus the GPS L1CA, which for the same chip length ($\approx 1\mu s$), the Galileo signal has 4 ms of period while the GPS L1CA signal period is 1ms.

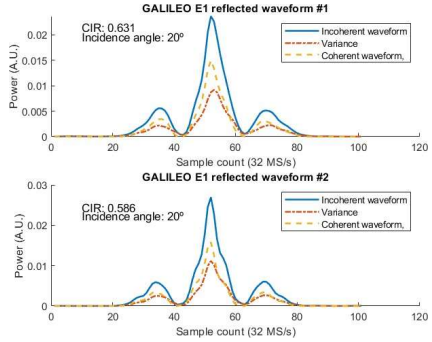

Fig. 3: Incoherent component, variance, and coherent component of Galileo E1 reflected signal

The next two signals, GPS L5 and Galileo E5a, are both generated with the 10230 chips per ms, basically the chip length is 10 times shorter ($\sim 0.1\mu s$).

As seen in Fig. 4, the GPS L5 waveform presents a lower CIR as compared to the GPS L1CA case for similar incidence angle (comparing the second L1CA waveform with the first L5 waveform). In addition, the coherent component at L5

does not have a significant change due to the incidence angle, both waveforms present a very close CIR value with a difference in the incidence angle of $\sim 16^{o}$.

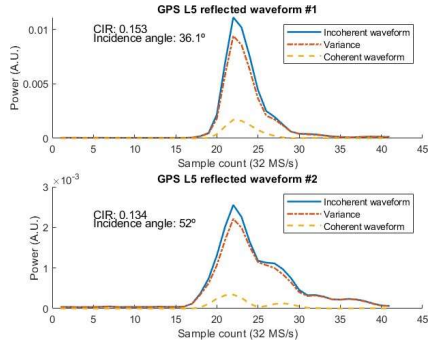

Fig. 4: Incoherent component, variance, and coherent component of GPS L5 reflected signal

Finally, Fig. 5 shows the same component untangling also for Galileo E5a reflected signal. The CIR value for this case is the same as in GPS L5 case, despite the incidence angle of 20°, reinforcing that the incidence angle and the CIR ratio at L5/E5a do not have any relation or that the CIR in the L5/E5a case is limited by the nature of the signal (i.e. the chip length).

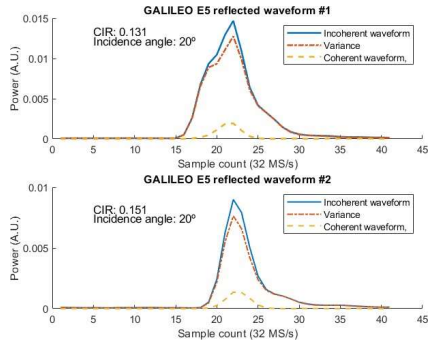

Fig. 5: Incoherent component, variance, and coherent component of Galielo E5a reflected signal

In addition to the detailed waveform analysis presented, the whole set of data has been processed following the proposed algorithm. The CIR evolution together with the incidence angle of the reflected signal is presented in Fig. 6 for the two beams of GPS L1CA and one beam of the E1 reflected signal. The CIR value is very noisy in all the three cases, and the mean and standard deviation are very close, indicating that the statistics of the CIR follow an exponential distribution. In the three cases, the mean is $\lambda \approx 0.19$ and the standard deviation $\sigma \approx 0.16$.

Analogously, for L5/E5a signals (Fig. 7), the CIR presents a very close mean and standard deviations, which also indicates the presence of an exponential distribution.

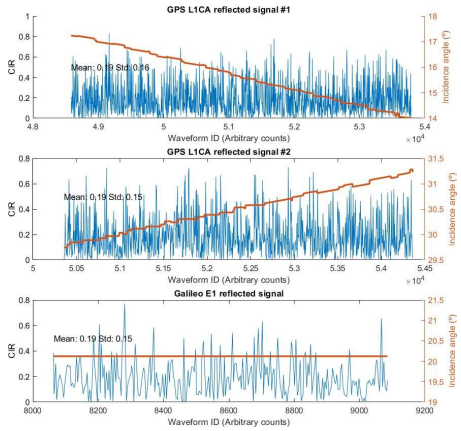

Fig. 6: Time evolution of GPS L1 and Galileo E1 reflected signals with different incidence angles

In the three cases, the mean is $\lambda \approx 0.03$ and the standard deviation $\sigma \approx 0.03$.

The CIR ratio between the L1/E1 and L5/E5a band is 6.33,

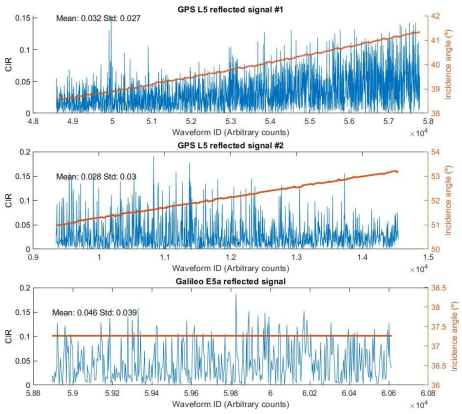

Fig. 7: Time evolution of GPS L5 and Galileo E5a reflected signals with different incidence angles

As an example of the data distribution, Fig. 8 shows the histogram of the GPS L1CA and GPS L5 data, where it is clearly identified the exponential distribution with different mean values depending on the band.

Comparing both L1/E1 and L5/E5a cases, there is a clear difference in the CIR ratio, which in principle does not depend on the incidence angle but on the characteristics of the signal itself, which may require further studies or analysis.

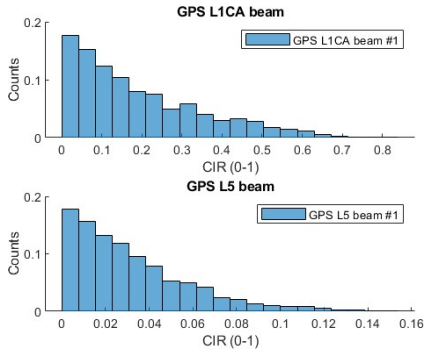

Fig. 8: Histogram of the reflected CIR of GPS L1CA and GPS L5 data

4. CONCLUSIONS

This paper has explained a technique to separate the coherent signal from the incoherent one on reflected GNSS signals from the sea surface, both for GPS and Galileo, at L1/E1 and L5/E5a bands. The results presented confirm the presence of a non-negligible coherent component in a reflection over the sea surface from an aircraft at 1500 m. height. An statistical analysis for its coherency ratio with respect to the incoherently averaged signal is also presented. The presented technique allows the processing of the coherent and incoherent components separately, which will improve the calibration accuracy, and increase the resolution of GNSS-R applications.

5. ACKNOWLEDGEMENTS

The data processing part of this work has been carried out by J.F. Munoz-Martin. The author wants to thank the project PI, A. Camps, for its support. The author also thanks all the other authors, which have contributed on the execution of the experiment. This work was supported by the Spanish Ministry of Science, Innovation and Universities, "Sensing with Pioneering Opportunistic Techniques", grant RTI2018-099008-B-C21, and the grant for recruitment of early-stage research staff FI-DGR 2015 and 2018 of the AGAUR - Generalitat de Catalunya (FEDER), Spain, and Unidad de Excelencia Mar´ıa de Maeztu MDM-2016-060.

6. REFERENCES

[1] H. Carreno-Luengo and A. Camps, "Unified GNSS-r formulation including coherent and incoherent scattering components," in *2016 IEEE International Geoscience and Remote Sensing Symposium (IGARSS)*. jul 2016, IEEE.

[2] V. U. Zavorotny and A. G. Voronovich, "Modeling signals of opportunity scattering from earth's surface with an improved bistatic radar equation," in *IGARSS 2018 - 2018 IEEE International Geoscience and Remote Sensing Symposium*, July 2018, pp. 235–238.

[3] F. Martin, A. Camps, F. Fabra, A. Rius, M. Martin-Neira, S. D'Addio, and A. Alonso, "Mitigation of direct signal cross-talk and study of the coherent component in GNSS-R," *IEEE Geoscience and Remote Sensing Letters*, vol. 12, no. 2, pp. 279–283, feb 2015.

[4] R. Onrubia, D. Pascual, H. Park, A. Camps, C. Rüdiger, J. Walker, and A. Monerris, "Satellite Cross-Talk Impact Analysis in Airborne Interferometric Global Navigation Satellite System-Reflectometry with the Microwave Interferometric Reflectometer," *Remote Sensing*, vol. 11, no. 9, pp. 1120, may 2019.

[5] R. Onrubia, D. Pascual, H. Park, and A. Camps, "Preliminary Altimetric and Scatterometric Results with the Microwave Interferometric Reflectometer (MIR) during its first airborne experiment," in *ARSI-KEO 2019, ESA, Noordwijk, Netherlands*.

[6] A. Camps, "Spatial resolution in gnss-r under coher- ent scattering," *IEEE Geoscience and Remote Sensing Letters*, vol. 17, no. 1, pp. 32–36, Jan 2020.

[7] D. Pascual, R. Onrubia, A. Alonso-Arroyo, H. Park, and A. Camps, "The microwave interferometric reflectometer. Part II: Back-end and processor descriptions," in *International Geoscience and Remote Sensing Symposium (IGARSS)*. jul 2014, pp. 3782–3785, IEEE.

[8] E. Valencia, a. Camps, J. F. Marchan-Hernandez, X. Bosch-Lluis, N. Rodriguez-Alvarez, and I. Ramos-Perez, "Advanced architectures for real-time Delay-Doppler Map GNSS-reflectometers: The GPS reflectometer instrument for PAU (griPAU)," *Advances in Space Research*, vol. 46, pp. 196–207, 2010.

[9] H. Carreno-Luengo, A. Amézaga, D. Vidal, R. Olivé, J.F. Munoz Martin, and A. Camps, "First Polarimet- ric GNSS-R Measurements from a Stratospheric Flightover Boreal Forests," *Remote Sensing*, vol. 7, pp. 13120–13138, 10 2015.

[10] V. U. Zavorotny, S. Gleason, E. Cardellach, and A. Camps, "Tutorial on remote sensing using gnss bistatic radar of opportunity," *IEEE Geoscience and Remote Sensing Magazine*, vol. 2, no. 4, pp. 8–45, Dec 2014.

[11] Joan Francesc Munoz-Martin, Raul Onrubia, Daniel Pascual, Hyuk Park, Adriano Camps, Christoph Rüdiger, Jeffrey Walker, and Alessandra Monerris, "Untangling the incoherent and coherent scattering components in gnss-r and novel applications," *Remote Sensing*, vol. 12, no. 7, 2020.